Transient temperature evolution of Selective Laser Melting process based on multilayer finite element model

Xiao Dongming[1], He Kuanfang[1], Wang Di[2]

(1. Engineering Research Center of Advanced Mine Equipment, Ministry of Education, Hunan University of Science and Technology, Xiangtan 411201, China;
2. School of Mechanical and Automotive Engineering, South China University of Technology, Guangzhou 510641, China)

Abstract: A multilayer transient temperature finite element model of Selective Laser Melting was established. This model took account of the temperature-material properties and the powder-to-solid transition by converting the powder thermophysical properties to the solid thermophysical properties. The FE model consisted of two layers of elements. The simulation results are in good agreement with the single track experiment result. The effects of scan speed (0.2 m/s, 0.4 m/s, 0.6 m/s) and laser power (80 W, 100 W, 120 W) on the temperature field were investigated. Simulation results show that the point of peak temperature slightly shifted toward the back of the laser beam rather than the center of laser beam when the laser beam moves. The peak temperature as well as the thermal gradient increases with increasing laser power and decreasing scan speed.

Key words: additive manufacturing; Selective Laser Melting(SLM); temperature field; multilayer FEA model

CLC number: TH164 **Document code:** A **Article ID:** 1007-2276(2015)09-2672-07

基于多层有限元模型的激光选区熔化多层瞬态温度场演化规律研究

肖冬明[1],何宽芳[1],王 迪[2]

(1. 湖南科技大学 先进矿山装备教育部工程研究中心,湖南 湘潭 411201;
2. 华南理工大学 机械与汽车工程学院,广东 广州 510641)

摘 要: 建立了激光选区熔化(SLM)加工的多层瞬态热有限元模型,该模型考虑了随温度变化的材料属性,并通过将粉末材料的热物理属性转换为实体材料的热物理属性来模拟粉末-实体的转换过程,有限元分析结果与单熔道实验结果吻合,验证了该模型的有效性。研究了扫描速度(0.2 m/s,0.4 m/s,0.6 m/s)和激光功率(80 W,100 W,120 W)对温度场的影响,并研究了相邻层之间的铺粉过程的冷却效应。结果显示,当扫描速度越大时,温度峰值点相较激光光斑中心越偏后,温度峰值和温度梯度随着激光功率的增大或者扫描速度的减小而增大,该研究为 SLM 加工工艺参数的选择提供了理论依据。

关键词: 增材制造; 激光选区熔化; 温度场; 多层有限元模型

收稿日期:2015-01-13; **修订日期:**2015-02-20

基金项目:国家自然科学基金(51405156);湖南省科技计划(2014FJ4265);湖南省教育厅科研项目(14C0432)

作者简介:肖冬明(1980-),男,讲师,博士,主要从事激光增材制造(3D 打印)方面的研究。Email:dominic741@163.com

0 Introduction

Selective Laser Melting (SLM) is one of the Additive Manufacturing (AM) technologies, which can directly fabricate complex metal parts from virtual CAD models using various metal powder materials. Metal powder experienced a process of powder-liquid-solid phase transition in a very short time during the SLM process. Large temperature gradient and uneven temperature distribution leads to stress cracking and warpage of parts in solidification process[1]. It is difficult to obtain transient temperature distribution with experimental means. Therefore, researchers generally use numerical simulation to study the temperature distribution. Wang[2] studied the relationship between energy input and melted track. It is found that the more energy input, the wider of the melted track and less risk of balling phenomenon. Craeghsa[3] tried to measure the temperature during the SLM process, but the results were not satisfactory. Finite Element Method(FEM) has recently been employed to perform temperature field analysis of the AM process. Shiomi[4] developed a thermal model to calculate temperature and stress distribution for various track lengths. Their research suggests that the cracking of layer can be avoided by using smaller track length. Hussein[5] built a FEM to investigate the temperature and stress fields in single layer. They found that the temperature deposited on powder bed is different on a solid substrate. Because the solid bulk materials have higher conductivity compared to powder bed. Matsumoto[6] developed a two-dimensional model to calculate the temperature and residual stress distribution during SLM process. They found that the scan strategy has great influence on the residual stresses, and using sector scan strategy can reduce deformation of the parts. Contuzzi[7] established a 3D thermal finite element model to evaluate the influences of SLM process parameters on the temperature distribution, but the thermochemical properties were temperature independent. Li[8] established a 3D finite element model to predict the width of track versus the process parameters, such as laser power, scan speed and scan interval. Zeng[9] used a new faster dynamic meshing method to solve thermal modelling.

Although some models have been proposed to investigate the temperature distribution in SLM process and got good insight into the mechanism of SLM process. However, the temperature distribution and their influences between contiguous layers have seldom researched. And some research ignored the transformation between powder thermophysical properties and solid thermophysical properties. These will lead to that the simulation results have insufficiency persuasion.

This study developed a multilayer thermal 3D FE model which included the effects of moving Gaussian heat source as well as temperature-dependent materials. The impacts of process parameters as well as the recoating time between the two layers on the temperature field of both layers were investigated.

1 Model description

1.1 Physical model of SLM process

Direct manufacturing of metal powder by SLM is a nonlinear thermal process. The heat transfer process follows the Fourier Heat Conduction Theory:

$$\lambda\left(\frac{\partial^2 T}{\partial x^2}+\frac{\partial^2 T}{\partial y^2}+\frac{\partial^2 T}{\partial z^2}\right)+q=\rho(T)C(T)\frac{\partial T}{\partial t} \tag{1}$$

where λ is the conductivity coefficient; T is the temperature; q is the internal heat; $\rho(T)$ is the density; $C(T)$ is the heat capacity coefficient.

Initial condition

$$T(x,y,z)=T_0,\ (x,y,z)\in D \tag{2}$$

where T_0 is the initial temperature; D is the scanned region.

Boundary condition

During the SLM process, laser irradiates the metal powder bed and forms a molten pool. It involves thermal conduction, thermal convection and thermal radiation.

$$-\lambda\frac{\partial T}{\partial n}=h(T-T_0)+\varepsilon_\theta\sigma(T^4-T_0^4) \tag{3}$$

where ε_θ is the thermal radiation coefficient; σ is the Stefan-Boltzmann constant, and h is the convection heat transfer coefficient. It assumes that the ambient temperature is equal to initial temperature.

Latent heat is taken into account for fusion and fluid flow of melt pool in SLM process. To account for the latent heat, enthalpy of the metal powder can be calculated as follow:

$$H(T)=\int \rho(T)C(T)\mathrm{d}T \tag{4}$$

1.2 3D finite element model of SLM process

The dimensions of the entire model developed in this study are 1.2 mm×1.2 mm×0.4 mm.

It consists of two parts: an underneath substrate and upside metal powder bed. The dimensions of substrate are 1.2 mm×1.2 mm×0.32 mm and powder bed are 1.2 mm×1.2 mm×0.08 mm. The layer of substrate is meshed by 8-node hexahedrons element with dimensions of 0.04 mm×0.04 mm×0.08 mm, while the powder bed is meshed by the dimensions of 0.04 mm×0.04 mm×0.02 mm. The powder bed is composited with two layers, each layer consists of two layers of elements, as shown in Fig.1. The dimensions of the scan region are 0.88 mm×0.88 mm.

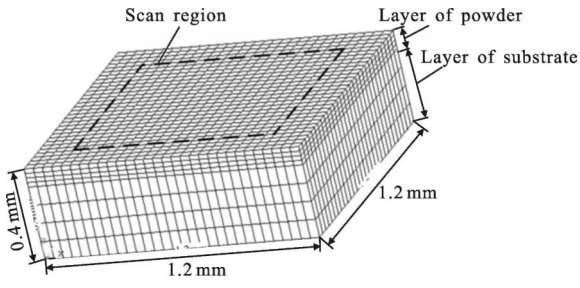

Fig.1 3D finite element model in SLM process

1.3 Moving Gauss heat source

The Gauss Heat Source is the most widely used in the finite element model of AM process. The laser energy is inputted in the powder bed in the form of thermal flux, it can be described as follow:

$$q=\frac{2AP}{\pi\omega^2}\exp(-2r^2/\omega^2) \tag{5}$$

where q is the thermal flux, A is the absorptivity of laser energy, P is the laser power, ω is the laser beam radius, r is the distance from a point in the irradiation area to the center of laser beam, it can be defined as:

The first layer:

$$r^2=(x-x_0-vt)^2+(y-y_0)^2 \tag{6}$$

The second layer:

$$r^2=(x-x_0)^2+(y-y_0-vt)^2 \tag{7}$$

where (x_0,y_0) is a point in the irradiation area on the surface of power bed.

In this study, the FE model of heat source is shown in Fig.2, the area of laser beam is assumed to be 8×8 elements.

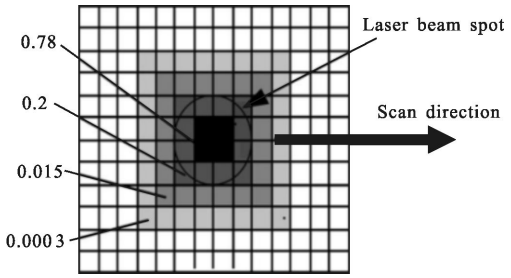

Fig.2. FE model of Gauss heat source

1.4 Materials properties

AISI 316L stainless steel powder is used in this simulation. The average particle is about 17 μm and the maximum particle size is 35 μm. Packed density is about 4.42 g/cm^3. The chemical compositions of 316L stainless steel are shown in Tab.1.

Tab.1 Chemical compositions of 316L stainless steel

Chemical compositions	C	Cr	Ni	Mo	Si	Mn	O	Fe
Mass fraction	0.03%	17.53%	12.06%	2.16%	0.86%	0.38%	0.13%	Bal

Gusarov[10] found that the thermal conductivity of powder materials plays an important role in the process of heat transfer, especially when the temperature of the material nears the Melting Temperature T_M. When the temperature is lower than the Solidus Temperature T_S, the Sih Model can be adopted to calculate the effective thermal conductivity λ_e:

$$\frac{\lambda_e}{\lambda_g}=(1-\sqrt{1-\phi})\left(1+\frac{\phi\lambda_r}{\lambda_g}\right)+\sqrt{1-\phi}\left(\frac{2}{1-\frac{\lambda_g}{\lambda_s}}\left(\frac{1}{\left(1-\frac{\lambda_g}{\lambda_s}\right)^2}\ln\left(\frac{\lambda_s}{\lambda_g}\right)-1\right)+\frac{\lambda_r}{\lambda_g}\right) \quad (8)$$

where λ_g and λ_s are the thermal conductivity of gas atmosphere and solid materials, ϕ is the porosity of the powder bed, λ_r is equal to:

$$\lambda_r=4F\sigma T^3D \quad (9)$$

where D is the mean diameter of powder particle, F is a view factor which is approximately taken as 1/3.

When the temperature is between the Solidus Temperature T_S and Liquidus Temperature T_L, the effective conductivity can be described as follow:

$$\lambda_e(T)=\lambda_g(T)+\rho_r^4(\lambda_s(T)-\lambda_g(T)) \quad T_S\leqslant T\leqslant T_L \quad (10)$$

where ρ_r is the relative density, it can be described as:

$$\rho_r=1-\varepsilon(T) \quad (11)$$

$\varepsilon(T)$ is the porosity of powder materials that changes from ε_0 to 0, linearly with temperature rises from Solidus Temperature to the Liquidus Temperature. It assumed that when temperature is below the Solidus Temperature, ε is a constant as ε_0.

This model took account of the powder-to-solid transition by converting the powder thermophysical properties to the solid thermophysical properties[11].

2 Model validation

In order to verify the suitability of the FE model, a comparative study with the experiment work was conducted on Demetal −100, which was a SLM workstation with a maximum laser power 200 W continuous wavelength of 1 090 nm fiber laser. The building envelop is 100 mm×100 mm×120 mm.

A series of single track pool are processed with fixed laser power of 100 W and various scan speed of 0.2 m/s, 0.4 m/s and 0.6 m/s, the powder is AISI 316 stainless steel. The single track pools are shown in Fig.3(a), their width respectively are 191 μm, 157 μm and 136μm. Figure 3(b) shows the predicted widths of single track pools varies from 197 μm, 161 μm, 125 μm. Figure 3 (c) shows the comparison of pool widths between the simulation and experiment. It shows that the width decreases with increasing scan speed, and the simulation results are in good agreement with the experiment one.

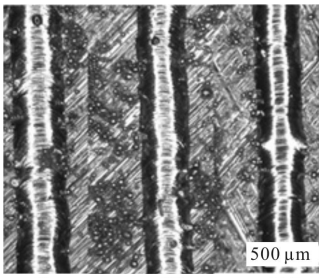

(a) Single scan track width versus scan speed

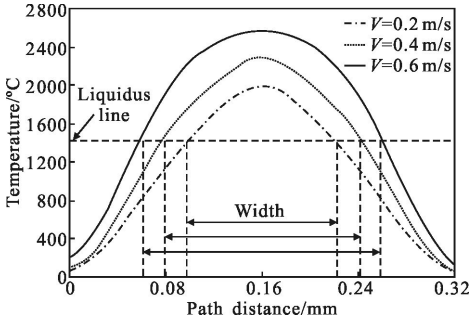

(b) Temperature distribution along route L

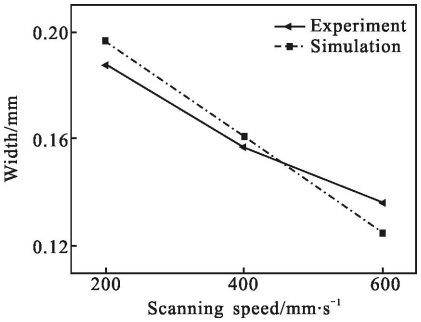

(c) Comparison of pool widths

Fig.3 Single scan track width of the SLM process

3 Results and discussions

The temperature distribution during the laser exposure and recoating time between contiguous layers have been investigated, it focuses on the effects of various processing parameters, including laser power, scan speed and the cooling time, because these parameters play important roles on processing quality. Besides, the fixed scan spacing is 0.08 mm, laser beam diameter is 0.16 mm, layer thickness is 0.04 mm,

the two different scan paths are used between contiguous layers, the first layer is along the X−axis, and the second layer is along the Y−axis, as shown in Fig.4(a) and (b).

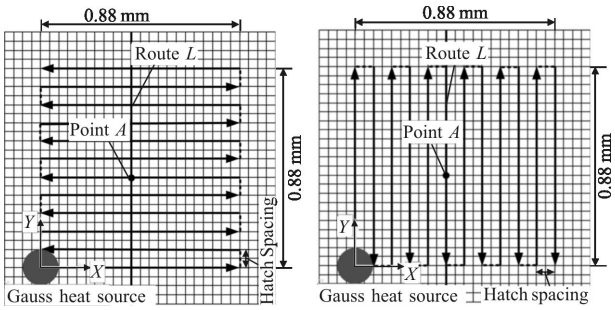

(a) X−axis direction of the first layer (b) Y−axis direction of the second layer

Fig.4 Scan patterns of the SLM process

3.1 Effect of scan speed

Figure 5 shows the temperature distribution along the route L of the first and second layer. The fixed laser power is 100 W, and the scan speed varies from 0.2 m/s to 0.6 m/s. The temperature curves of 0.2 m/s, 0.4m/s and 0.6 m/s are respectively named curve $C1$, $C2$ and $C3$. The curves are divided into three segments and named $L1$, $L2$ and $L3$.

Figure 5 (a) shows the effect of scan speed on the temperature distribution along the route L of the first layer when the laser beam irradiates at the point A. The elements lying on the segment $L1$ have been solidified due to the laser irradiating, and elements lying on segment $L2$ are under the laser exposure, while $L3$ represents the area that has not been irradiated yet. Within the $L1$, temperature of the curve $C1$ is far lower than that of $C2$ and $C3$, while exceeds that of $C2$ and $C3$ within segment $L2$. That is because with high scan speed, the interval time between two continuous scan tracks is short. The heat due to the laser beam irradiating conducted insufficiently to the surrounding elements, so the nodal temperature on the former track remains high level during the short interval time.

Figure 5 (b) shows the temperature curves of the second layer along route L. The current scan track coincides with the route L. Elements on segment $L1$ are not irradiated by the laser beam, but the temperature are higher than the ambient temperature as well as the curve $C1$ is higher than that of curves $C2$ and $C3$. This discrepancy could be attributed to the fact of prolonging laser treatment at a low scan speed, it let more heat conduct to adjacent elements. Within segment $L2$, the peak temperatures are not found at the center of the laser beam, but slightly shifted toward the back of the laser beam, especially when the laser beam moves at the high scan speed, such as 0.6 m/s. This phenomenon can be ascribed to the fact that higher scan speed means less interaction time between laser beam and powder. The heat conducted insufficiently to surrounding elements when laser beam moves from one point to next.

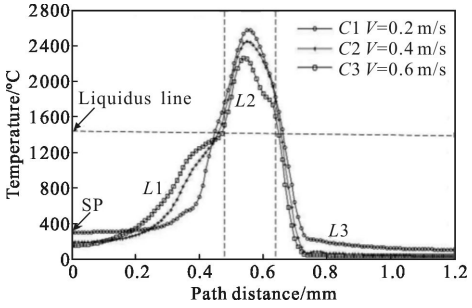

(a) First layer

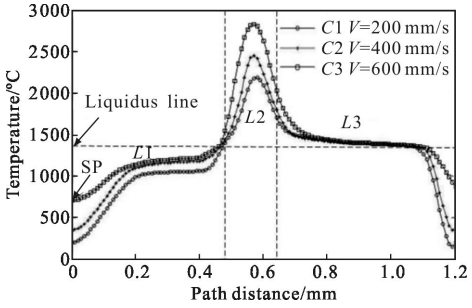

(b) Second layer

Fig.5 Temperature distribution with different scan speed along the route L

3.2 Effect of the laser power

Figure 6 shows the effect of laser power on temperature distribution along the route L, with a fixed scan speed of 400 mm/s but different laser power of 80 W, 100 W and 120 W. Their curves are respectively named curve $C1$, $C2$ and $C3$, every curve

are divided into three segmen ts and named *L*1, *L*2 and *L*3.

Figure 6 (a) shows the effect of laser power on temperature distribution of the first layer along the route *L* when laser beam irradiates at the point *A*. Unlike Fig.5 (a), the trend of the three curves within segment *L*1 are highly similar. The elements lying on segment *L*2 are under the laser exposure, the maximum temperature are 2 220 ℃, 2 674 ℃ and 2 771 ℃, while the maximum temperature gradients are respectively 10.7 ℃/μm, 18.6 ℃/μm and 17.2 ℃/μm. Unlike the maximum temperature, the maximum temperature gradients are nonlinear. This is because the heat-affected zone of the previous track with high laser power is larger than that with low laser power, and the elements lying on the current track are preheated.

Figure 6 (b) shows the temperature curves of the second layer along route *L* with different laser power of 80 W, 100 W and 120 W. The elements lying on segment *L*1 have not yet been irradiated by the laser beam, and elements lying on segment *L*2 are under the laser exposure, while *L*3 represents the area that have been solidified due to the laser irradiating. Compared the three curves, it is found that when laser power increases from 80 W to 120 W, the thermal gradient are respectively 12.2 ℃/μm, 14.3 ℃/μm and 15.9 ℃/μm within segment *L*2. The reason is that the temperature of molten pool increases with increasing laser power, while the elements that surrounding the molten pool are powder phase, they conduct heat slowly to their surrounding elements.

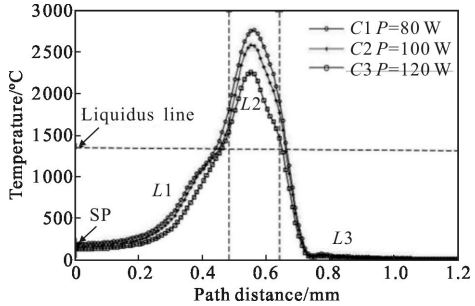

(a) First layer

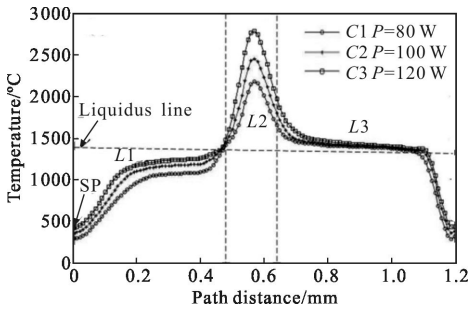

(b) Second layer

Fig.6 Temperature distribution with different laser power along the route *L*

4 Conclusions

A multilayer finite element model including the effect of the powder-to-solid transition was established to investigate the transient temperature evolution in SLM process. This model considered the temperature-dependent material properties, such as thermal conductivity, convection, radiation and density. The effects of laser power and scan speed on temperature distribution during the processing have been investigated. We got the following conclusions:

The trend of the temperature distribution curves along route *L* with increasing laser power and decreasing scan speed are similar. The peak temperature as well as the thermal gradient increases with increasing laser power and decreasing scan speed. The simulation results imply that preheating can decrease thermal gradient efficiently.

The point of peak temperature slightly shifted toward the back of the laser beam rather than at the center of laser beam when the laser beam moves at a high scan speed. Simulation and experiment results show that the scan track width getting narrow down linearly when scan speed increases linearly.

References:

[1] Kruth J P, Deckers J, Yasa E, et al. Assessing and comparing influencing factors of residual stresses in selective laser melting using a novel analysis method [J]. ***Journal of Engineering Manufacture***, 2012, 226(6): 980−991.

[2] Wang D, Yang Y, Su X, et al. Study on energy input and

its influences on single-track, multi-track, and multi-layer in SLM [J]. ***The International Journal of Advanced Manufacturing Technology***, 2012, 58(9-12): 1189-1199.

[3] Craeghs T, Bechmann F, Berumen S, et al. Feedback control of Layerwise Laser Melting using optical sensors [J]. ***Physics Procedia***, 2010, 5: 505-514.

[4] Shiomi M, Yoshidome A, Abe F, et al. Finite element analysis of melting and solidifying processes in laser rapid prototyping of metallic powders[J]. ***International Journal of Machine Tools and Manufacture***, 1999, 39(2): 237-252.

[5] Hussein A, Hao L, Yan C, et al. Finite element simulation of the temperature and stress fields in single layers built without-support in selective laser melting [J]. ***Materials & Design***, 2013, 52: 638-647.

[6] Matsumoto M, Shiomi M, Osakada K, et al. Finite element analysis of single layer forming on metallic powder bed in rapid prototyping by selective laser processing [J]. ***International Journal of Machine Tools and Manufacture***, 2002, 42(1): 61-67.

[7] Contuzzi N, Campanelli S L, Ludovico A D. 3D finite element analysis in the selective laser melting process[J].***International Journal of Simulation Modelling***, 2011, 10(3): 113-121.

[8] Li R, Shi Y, Liu J, et al. Effects of processing parameters on the temperature field of selective laser melting metal powder [J]. ***Powder Metallurgy and Metal Ceramics***, 2009, 48(3-4): 186-195.

[9] Zeng K, Pal D, Gong H J, et al. Comparison of 3DSIM thermal modelling of selective laser melting using new dynamic meshing method to ANSYS [J]. ***Materials Science and Technology***, 2015, 31(8): 945-956.

[10] Gusarov A V, Yadroitsev I, Bertrand P, et al. Heat transfer modelling and stability analysis of selective laser melting[J]. ***Applied Surface Science***, 2007, 254(4): 975-979.

[11] Dai K, Shaw L. Finite element analysis of the effect of volume shrinkage during laser densification [J]. ***Acta Materialia***, 2005, 53(18): 4743-4754.